Available online at www.sciencedirect.com
ScienceDirect
Catalysis Today 126 (2007) 3–17
CATALYSIS TODAY
www.elsevier.com/locate/cattod

A surface science approach to ambient pressure catalytic reactions

Günther Rupprechter *

Institute of Materials Chemistry, Vienna University of Technology, Veterinärplatz 1, A-1210 Vienna, Austria

Available online 7 January 2007

Abstract

Recent advances in the preparation and characterization of planar model catalysts and in ambient pressure surface spectroscopy enable us to investigate well-defined supported metal nanoparticles under working conditions, approaching the conditions of applied catalysis. The reactivity of Pd–Al_2O_3/NiAl(1 1 0) model catalysts for CO hydrogenation and methanol partial oxidation were examined by sum frequency generation (SFG) vibrational spectroscopy and by polarization-modulation infrared reflection absorption spectroscopy (PM-IRAS) at pressures ranging from ultrahigh vacuum to ~1 bar. Kinetic measurements were performed by on-line gas chromatography. A comparison with Pd(1 1 1) revealed the inherent differences between Pd nanoparticles and Pd single crystals. Apart from differences in surface structure, the small volume (or finite size) of Pd nanoparticles strongly affected their properties, in particular for hydrogen absorption. Methanol oxidation proceeded via dehydrogenation to formaldehyde CH_2O, which either desorbed or further dehydrogenated to CO, which was subsequently oxidized to CO_2. Carbonaceous overlayers that were present during the reaction were shown to favourably affect the selectivity towards CH_2O. During methanol oxidation Pd particles were more easily oxidized than Pd(1 1 1), which reduced their activity. Deactivation of Pd nanoparticles supported on Nb_2O_5/Cu_3Au(1 0 0), a support less inert than alumina, originated from the formation of mixed ''Pd–NbOx'' sites. 1,3-butadiene hydrogenation is known to be particle size dependent but when a realistic structural model of Pd nanoparticles on alumina was used for rate normalization, the reaction turned out to be particle size independent, even though the reaction is structure-sensitive, as corroborated by reactivity studies on Pd single crystals.

Keywords: Palladium; Nanoparticles; Alumina; Niobia; Carbon monoxide; Hydrogen; Methanol; Butadiene; Hydrogenation; Oxidation; Low index single crystal surfaces; Catalysis; Vibrations of adsorbed molecules; Model catalysts

1. Introduction

Model Catalysis has come a long way. For many years surface science studies of catalytic processes have been nearly exclusively performed on transition and noble metal single crystals ([1–4] and references therein). Although these studies have elucidated many elementary steps of catalytic reactions, the single crystal approach carries inherent deficiencies. For instance, the absence of nano-sized (metal) particles or of an oxide support makes it difficult to extrapolate surface science results to technological supported metal catalysts. First attempts to overcome this so called ''materials gap'' involved the growth of oxide islands on metal substrates (''inverse catalysts'' [1,5,6]) but significant advances were based on the development of planar nanoparticle model catalysts, consisting of well-defined metal particles supported on thin oxide films or on oxide single crystals [7–15]. The preparation of planar model systems under ultrahigh vacuum (UHV) using ultra pure materials guarantees the absence of undesired elements that are sometimes difficult to avoid (and detect) for conventional catalysts. The mean particle size (~1–10 nm) as well as the particle morphology and defect structure can be accurately controlled (cf. Fig. 1) and the planarity and electrical and thermal conductivity of the model systems allows applying a wide range of surface sensitive imaging (e.g. scanning tunneling microscopy, STM) and spectroscopic (e.g. X-ray photoelectron spectroscopy, XPS; infrared reflection absorption spectroscopy, IRAS; sum frequency generation, SFG; temperature programmed desorption, TPD, etc.) techniques. To date, an increasing number of technical catalysts can be mimicked and various combinations of Pd, Pt, Rh, Ag, Au, bimetallic (Pd/Co, Pd/Ag, Pd/Au), etc nanoparticles supported by Al_2O_3, SiO_2, TiO_2, Fe_3O_4, Nb_2O_5, MgO, etc., have been examined (see e.g. [16,17] and references therein).

* Tel.: +43 1 25077 3813; fax: +43 1 25077 3890.
E-mail address: grupp@imc.tuwien.ac.at.

0920-5861/$ – see front matter © 2007 Elsevier B.V. All rights reserved.
doi:10.1016/j.cattod.2006.12.005

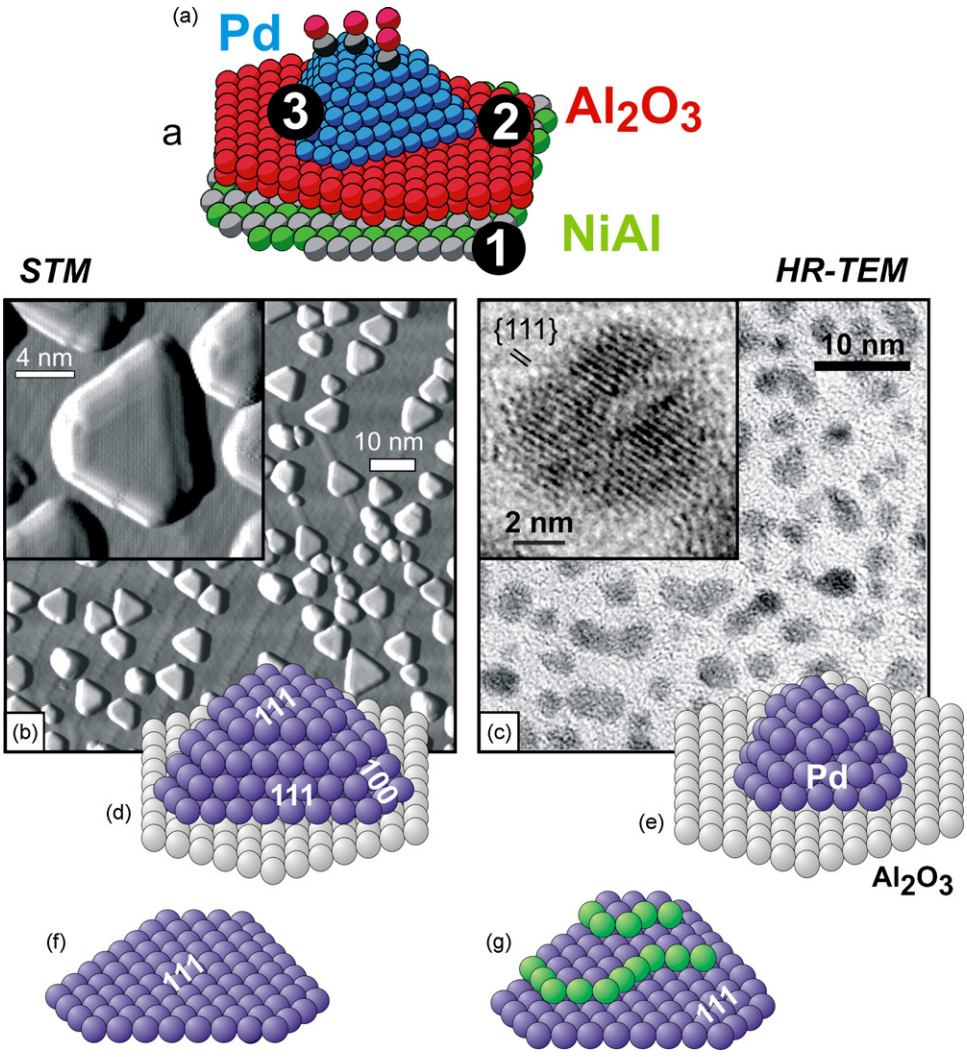

Fig. 1. (a) Graphical illustration of the preparation of Pd nanoparticles supported by Al_2O_3/NiAl(1 1 0) and of Pd model catalysts with various (surface) morphologies: (b) STM image (100 nm × 100 nm, adapted from [45,46]) and (c) HRTEM image of Pd nanoparticles, grown at 300 K and 90 K, respectively. The insets show individual particles at higher magnification. Controlling the growth conditions allows preparing Pd particles with different morphology/surface structure, for instance well-faceted truncated cuboctahedra (d) or rougher, defective particles (e). Single crystal surfaces that were used for comparison are also shown: (f) well-ordered Pd(1 1 1) and (g) a ''defect-rich'' (ion-bombarded) Pd(1 1 1).

Despite the success in the development of model catalyst, studies of their catalytic activity under UHV (e.g. by TPD) are typically very different from the conditions of isothermal, steady state ambient pressure catalytic tests of technical catalysts. Molecular beam studies are probably the best approach to examine reaction kinetics on model catalysts under UHV [18], but due to pressure limitations (operating pressure typically $<10^{-6}$ mbar) the surface coverages may be lower than in the real catalytic process (especially for reactions at elevated temperature), leading to different adsorption site populations. These considerations illustrate the so-called ''pressure gap'' between surface science and applied catalysis. To circumvent this gap, efforts have been devoted to develop UHV-compatible high-pressure reaction cells and to carry out surface characterization/spectroscopy under non-UHV conditions, i.e. under mbar to atmospheric pressure [17,19–24]. Photon-based methods such as sum frequency generation (SFG) vibrational spectroscopy or polarization-modulation infrared reflection absorption spectroscopy (PM-IRAS) [17], together with high-pressure X-ray photoelectron spectroscopy (HP-XPS) [25–29] and high-pressure scanning tunneling microscopy (HP-STM) [30–33] are currently among the prime techniques for *in situ* studies of catalytically active surfaces (monitoring ''model catalysts at work'').[1] Despite the nano-hype one should not forget, however, that studies on single crystals as well as ''classical'' UHV experiments are still inevitable to interpret and quantify the ambient pressure results.

Combining nanoparticle model catalysts with *in situ* surface spectroscopy at elevated pressure, utilizing suitable UHV systems equipped with high-pressure reaction cells, which are

[1] Here we avoid the term ''operando'' [34], which refers to simultaneous spectroscopic and kinetic measurements, because ''operando'' also implies that technically applied reactor types are used (which is not the case for UHV-high pressure cells of model studies).

connected to on-line gas chromatography for simultaneous kinetic measurements, thus allows monitoring catalytic reactions under conditions approaching technical systems. A number of case studies is presented below, including CO adsorption and hydrogenation and partial methanol oxidation, carried out on Pd–Al_2O_3 model catalysts as well as on Pd(1 1 1) single crystals. Parts of these investigations have been presented in previous articles; here we attempt a synopsis of the experimental and theoretical results, providing a broader, more comprehensive view. Finally, more complex catalysts (metal–support interaction on Pd–Nb_2O_5) and more complex reactions (selective 1,3-butadiene hydrogenation) will be briefly discussed as examples for future model catalysis research.

2. Model catalysts and spectroscopy under reaction conditions

2.1. Model catalyst surfaces: supported nanoparticles and single crystals

Thin Al_2O_3 films grown on NiAl(1 1 0) have turned out to be well-suited model supports. The preparation, structure, adsorption and catalytic properties of Al_2O_3/NiAl(1 1 0) have been thoroughly explored by Freund and coworkers [10,35–38], but have also attracted the attention of other groups [39–43]. As schematically shown in Fig. 1, a thin well-ordered Al_2O_3 model support is grown by oxidation of a NiAl(1 1 0) alloy single crystal (10^{-5} mbar O_2 at 523 K). The structure of the alumina film was examined by a variety of techniques ([37] and references therein) and recently it was even possible to image its atomic structure by low-temperature (4 K) STM [43,44]. The alumina film is only ~0.5 nm thick, hydroxyl-free and one should also keep in mind that its exact structure may deviate from bulk aluminas [37,41,42]. Its properties are certainly influenced by the observed line defects (antiphase domain boundaries and reflection domain boundaries) [43,44] but this is not treated in detail here.

One can certainly argue that the absence of hydroxyl groups on the alumina films used for the studies described below somewhat limits their relevance for catalysis. One can hardly argue against that but, nevertheless, the current alumina films provide a well-defined and rather inert substrate for the growth of well-shaped Pd nanoparticles, which is the basis for a comparison with Pd single crystals. Furthermore, as discussed below, a comparison with technological catalysts shows that the model systems mimic a real catalyst quite well.

Appropriate control of the growth parameters allows preparing Pd nanoparticles with different morphology and surface structure, as displayed in Fig. 1. Pd was deposited on the Al_2O_3 film either at 300 or 90 K (Pd amount equal to a nominal thickness of 2 ML). STM [36,39,45,46] indicated that the Pd particles grow preferentially along line defects at 300 K (nucleation density $\sim 1 \times 10^{12}$ particles/cm^2; Fig. 1b), whereas at 90 K the reduced Pd mobility leads to a higher nucleation density and thus to a more homogeneous distribution (nucleation density $\sim 5 \times 10^{12}$ particles/cm^2; Fig. 1c). The Al_2O_3 temperature during Pd deposition also influenced the particle morphology. Pd particles grown at 90 K had a mean size of 3.5 nm and were of rounded (irregular, maybe hemispherical) shape (about 850 atoms/particle; ca. 300 surface atoms). No high-resolution STM images could be obtained but TEM suggested a high number of low-coordination sites (defects, steps, etc.; cf. inset in Fig. 1c [47]). Pd particles grown at 300 K had a mean size of 6 nm and were of cuboctahedral shape (about 3000 atoms/particle; ca. 600 surface atoms; cf. inset in Fig. 1b). According to atomically resolved STM images the particles exhibit a (1 1 1) top facet and (1 1 1) and (1 0 0) side facets [39] with the (1 1 1) facets comprising about 80% of the particle surface (and with the remaining ~20% being (1 0 0) facets). The Pd particles were ''stabilized'' as described in [48] to increase their thermal stability up to ~600 K. Fig. 1 also shows models of Pd(1 1 1) and stepped (ion-bombarded; ''defect-rich'') Pd(1 1 1) single crystal surfaces which were used as reference samples [49,50]. One should also note that the successful preparation of well-defined nanoparticles and their thorough characterization has also been achieved under conditions that are more similar to those of technical catalysis (see e.g. [15,51–58]).

2.2. Ambient pressure surface sensitive techniques

It is well documented that the state of a catalyst under working conditions, i.e. in the presence of reactants and products at a high reaction temperature, may be different from what is observed by surface studies before and after a reaction under UHV at cryogenic temperatures [59,60]. These differences may be related to pressure- or temperature-induced changes of the binding configurations of the adsorbed species and/or to changes of the surface structure/composition of the catalyst (with both effects being correlated). Pre- and post-reaction characterization may certainly reveal pronounced changes of a catalyst such as particle sintering or alterations in composition, but characteristics of a catalyst that are inherently connected to its working state are not detected. How much could one tell about a soccer match by visiting the stadium before and after the game? One would watch spectators while the active players were absent.[2] In order to identify reaction mechanisms, catalysts should therefore ideally be characterized under operating conditions. For model catalysts, structure can be determined *in situ* by HP-STM, catalyst composition by HP-XPS, and the interaction with gas molecules by SFG or PM-IRAS (and other methods like surface X-ray diffraction, XRD). Accordingly, for technological catalysts one would apply environmental transmission electron microscopy (ETEM) [61–63], HP-XPS, *in situ* FTIR, Raman, XRD, etc. Such an ambitious goal can typically only by achieved by close collaborations because one laboratory has hardly the expertise for all methods.

For the Pd–Al_2O_3/NiAl(1 1 0) and Pd(1 1 1) model catalysts, reaction conditions were selected such that strong structural

[2] One should not take this analogy too far but people being there before and after the reaction are like ''probe molecules'' that mark some of the ''available sites'', but still not those sites involved in the real action.

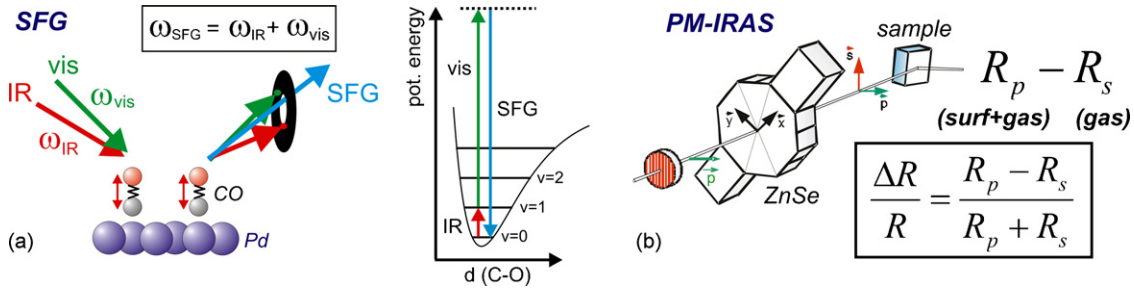

Fig. 2. High-pressure surface sensitive techniques: (a) IR–vis sum frequency generation (SFG) vibrational spectroscopy and (b) polarization-modulation infrared reflection absorption spectroscopy (PM-IRAS); adapted from [17,47] with permission from The Royal Society of Chemistry.

changes (like particle sintering or re-faceting) or compositional changes did not occur (in most cases), as indicated by imaging and spectroscopic analysis before and after the reaction. Our focus has therefore been on the characterization of the adsorbed/reacting molecules on the catalyst surface via vibrational spectroscopy. One has to confess, however, that this does not exclude reversible local changes of surface structure that may be present only under reaction conditions (e.g. by adsorbate-induced restructuring [1,4]).

Two "high-pressure" vibrational spectroscopies were applied, SFG and PM-IRAS (Fig. 2). Both methods are capable of characterizing adsorbed molecules or surface species independent of the gas pressure, and can be operated under UHV (which is important for comparison with "classical" surface science results) as well as at pressures up to 1 bar (for comparison with kinetic studies) [17]. The fundamentals of SFG [17,64–66] and PM-IRAS [67–74] have been discussed in a number of previous articles and only the most important aspects are repeated here.

To obtain an SFG vibrational spectrum, two (picosecond) laser beams are spatially and temporally overlapped on the adsorbate/substrate system (Fig. 2a). One beam is at fixed frequency (wavelength), e.g. at 532 nm, whereas the second beam is scanned in the mid-IR region. In case of a vibrational resonance of the adsorbate, a sum frequency signal is created, which is in the blue. Plotting the SFG intensity versus the IR wave number thus results in a vibrational spectrum. In a simple picture the SFG process is a combination of IR and anti-Stokes Raman and, in fact, a vibration must be simultaneously IR and Raman active to be SFG-active. Thus, an SFG signal is only created at the gas/surface interface and not in the gas phase, which makes SFG surface-specific.[3]

In contrast, PM-IRAS is not surface-specific but eliminates the gas phase absorption signal by polarization modulation of the incident IR light. As described by the metal surface selection rule [76], the effective surface intensity of s-polarized infrared light on a metal surface is basically zero and no surface absorption occurs. Thus, IR spectra acquired in s-polarization are IR gas phase spectra. In contrast, IR spectra acquired in p-polarization contain contributions of absorption of both surface and gas phase species. Polarization modulation is performed by a photoelastic modulator (ZnSe) at a frequency of 74 kHz and p- and s-spectra are thus acquired (nearly) simultaneously. After demodulation, (p − s) spectra are obtained characterizing the vibrational signature of the surface species (with only minor distortion by the gas phase). The s-spectra (or (p + s)-spectra which are basically identical due to the weakness of surface absorption) comprise the corresponding gas phase spectra.

Compared to SFG, PM-IRAS offers some advantages. First, PM-IRAS simultaneously monitors surface as well as gas phase absorptions. Second, whereas SFG is often limited to wave numbers higher than ~1600 cm^{-1} (due to a strong decrease of the IR intensity below 2000 cm^{-1}), the frequency range of PM-IRAS (ca. 800–4000+ cm^{-1}) allows additionally detecting deformation modes, fingerprinting signatures, etc. Third, PM-IRAS spectra may take a few minutes (for a scan 800–4000 cm^{-1}), whereas SFG acquisition times are typically on the order of 20 min (for a scan 1800–2200 cm^{-1}).[4] On the other hand, SFG allows performing time-resolved pump-probe experiments (with picosecond or even higher resolution) [79,80], as well as polarization-dependent measurements (e.g. [81,82]) determining the orientation of adsorbed molecules on a surface (for instance the tilt angle of specific bonds). The interpretation of signal intensities is not straightforward both for SFG and PM-IRAS, as described in detail in [83,84]. For both vibrational methods, calibration by HP-XPS or TPD should be carried out.

2.3. UHV-compatible high-pressure reaction cells

In order to perform ambient pressure spectroscopy on UHV-grown model catalysts, a dedicated apparatus is required, that combines a UHV preparation and surface analysis chamber with a UHV–high-pressure reaction cell that allows performing vibrational spectroscopy on the catalyst under working conditions [17,24,47,85]. Fig. 3 displays such a setup (for PM-IRAS) as well as the optical arrangement. The upper UHV section is equipped for sample preparation (ion sputtering for sample cleaning, leak valves for gas exposure, metal evaporators and quartz thickness monitors) and sample

[3] The gas phase pressure still indirectly affects the SFG process by IR absorption in the gas phase, an effect which must be accounted for by normalization of the SFG signal by the IR surface intensity [24,75].

[4] For "scanning SFG"; broadband SFG [77,78] spectra may take only a few minutes, but the IR range is typically limited to a few hundred wave numbers.

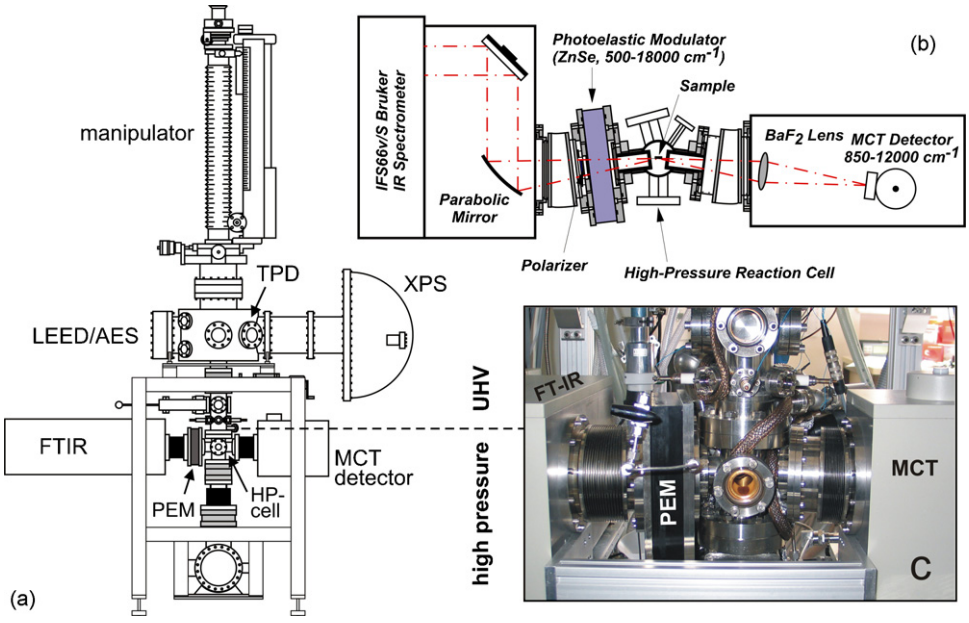

Fig. 3. (a) Experimental setup combining a UHV surface analysis chamber with a UHV–high-pressure reaction cell optimized for PM-IRAS spectroscopy. Pre- and post-reaction surface analysis under UHV can be performed by XPS, LEED, AES and TPD. The optical setup and the high-pressure reaction cell are shown in (b) and (c), respectively.

characterization (by LEED, AES, XPS, TPD), with the single crystal substrate mounted on an *xyzθ* manipulator. Using the manipulator a model catalyst can be transferred under UHV to the reaction cell. During this operation the sample holder is inserted into an arrangement of three differentially pumped spring-loaded Teflon seals and the reaction cell is separated from the UHV part [24]. Vibrational spectroscopy can then be performed in the reaction cell, either under UHV or at pressures up to 1 bar (the setup shown in Fig. 3 is equipped for PM-IRAS but the arrangement for SFG is very similar). The high-pressure cell is also interfaced to a gas chromatograph for product (gas phase) analysis during reaction studies.

A specific feature of this apparatus worth nothing is that it is able to perform ''true'' UHV experiments at low pressure/low temperature. Such experiments are often inevitable for signal calibration and for comparison with results obtained using conventional UHV systems. Smaller reaction cells can (and have!) certainly be constructed but at cost of vacuum and, thus, of cleanliness of the sample environment. For the current setup, sample transfer under UHV to the upper section allows for well-controlled post-reaction surface analysis.

3. Results

The interaction of Al_2O_3 supported Pd nanoparticles and Pd(1 1 1) with CO, hydrogen, methanol and oxygen was studied under a variety of conditions of pressure and temperature. This includes adsorption and coadsorption of the different reactants under UHV, and reactivity studies at mbar pressures, for temperatures ranging from 100 to 550 K. Various methods were applied (SFG, PM-IRAS, TPD, LEED, AES, XPS) and a comparison between results on Pd–Al_2O_3 and Pd(1 1 1) revealed the inherent differences between the properties of Pd nanoparticles and single crystals. Density functional theory (DFT) calculations were inevitable to interpret the vibrational data of adsorbed CO and to understand hydrogen absorption and CO–H coadsorption. Metal–support interaction occurred for Pd–Nb_2O_5 model catalysts and particle size effects were examined for ambient pressure 1,3-butadiene hydrogenation on Pd–Al_2O_3. In the following, the key experiments are discussed that helped to shine some light on reaction mechanisms.

3.1. CO adsorption, H adsorption and Pd-hydride formation, CO–H coadsorption and CO hydrogenation on Pd–Al_2O_3 and Pd(1 1 1)

The adsorption of CO on various Pd single crystal surfaces is well documented for UHV conditions (see references in [86]). Particularly, for Pd(1 1 1) the different CO adsorbate layers formed at increasing coverage and at various surface temperatures were studied by (nearly) every surface-specific method (LEED, AES, TPD, IRAS, HREELS, SFG, XPS, photoelectron diffraction, STM, DFT, etc). There is even a considerable number of ambient pressure studies by SFG and PM-IRAS [49,69,71,72]. In summary, all adsorbate structures observed, even those at ambient pressure, are comprised of the ''regular'' CO adsorption configurations, i.e. hollow-, bridge-, and linearly bonded CO. No indications for ''high-pressure species'' were found.

For supported Pd nanoparticles the situation is more complex. Vibrational spectra of CO adsorption are not just a superposition of single crystal spectra of the (1 1 1) and (1 0 0) particle facets [49,87,88]. Fig. 4a shows an SFG spectrum characterizing CO adsorption at 600 mbar/200 K on Pd nanoparticles. As mentioned, the Pd nanoparticles had the shape of flat, truncated cuboctahedra, with a mean diameter of ~6 nm (height: ~2 nm; ~3000 atoms/particle; ~600 surface

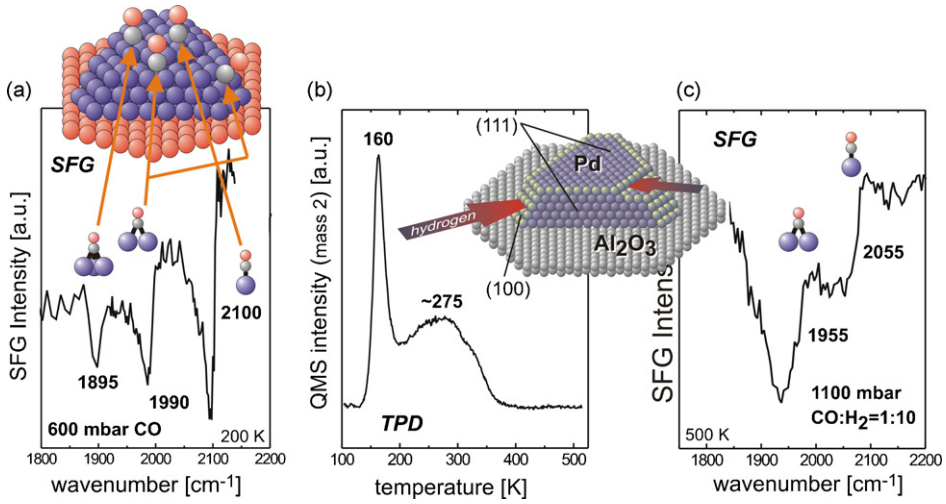

Fig. 4. (a) High-pressure SFG spectra of CO adsorbed on 6 nm Pd nanoparticles at 600 mbar and 200 K. (b) Thermal desorption spectra of hydrogen acquired after cooling Pd–Al_2O_3/NiAl(1 1 0) in 2×10^{-7} mbar H_2 from 300 to 100 K (~80 L). The model illustrates that Pd-hydride formation proceeds mainly via particle steps/edges and (1 0 0) facets. (c) High-pressure SFG spectra of a 1:10 CO/H_2 mixture on Pd–Al_2O_3 at 500 K [93].

atoms/particle; $\sim 1 \times 10^{12}$ particles/cm^2). About 80% of the particle surface consisted of (1 1 1) facets and the remaining 20% were mostly (1 0 0) facets. Similar morphologies were frequently reported for noble metal particles of technological catalysts, as observed by HRTEM [47,89,90].[5]

The SFG spectrum in Fig. 4a shows three peaks, at 1895, 1990, and 2100 cm^{-1} (and a shoulder at ~1965 cm^{-1} which is very weak in this spectrum). The spectrum is characteristic of a near saturation CO coverage. The peaks at 1895 and 2100 cm^{-1} are due to hollow and on-top CO on the (1 1 1) particle facets, respectively, similar to the (2×2)-3CO saturation structure on Pd(1 1 1) single crystals. In a similar way, one could assign the intense 1990 cm^{-1} peak to the (1 0 0) particle facets but its intensity is too high to originate exclusively from the (1 0 0) facets (comprising only 20% of the surface). An additional contribution to the 1990 cm^{-1} peak is due to CO bridge bonded to particle edges and steps, as corroborated by comparison with CO adsorption on stepped surfaces [49] and by DFT calculations [91]. Considering the particle shape, the (1 0 0) facets and the particle edges are "minority sites" (~20 and <10% of the surface atoms, respectively) and "intensity borrowing"[6] [76,87,92] from bridging CO on (1 1 1) facets (taking away intensity from the ~1965 cm^{-1} species) most likely enhances the 1990 cm^{-1} peak. The lineshape of the SFG spectra has been explained in detail elsewhere [83].

Hydrogen adsorption, absorption and Pd-hydride formation on Pd–Al_2O_3 have been investigated by TPD via the characteristic desorption temperatures (Fig. 4b; decomposition of Pd-hydride around 160 K; recombinative desorption of adsorbed hydrogen around 300 K [93]). It was demonstrated that Pd-hydride phases were more easily formed for Pd nanoparticles than for Pd(1 1 1) (or other low index single crystal surfaces), due to smaller surface to subsurface diffusion barriers at particle steps [86,93]. Such hydride phases (or bulk/subsurface hydrogen) have been proposed to exhibit a higher catalytic activity than adsorbed hydrogen but this issue is still under debate [93–96]. In any case, for the conditions of ambient pressure CO hydrogenation discussed below, the hydrogen pressure (1 bar) at the reaction temperature (500 K) is too low for the formation of β-Pd-hydride.

The coadsorption of CO and hydrogen was studied under UHV by combining SFG and TPD spectroscopy [86,93,97,98]. These experiments indicated that the resulting adsorbate layer strongly depended on (i) the type of gas dosing (sequential dosing of CO and hydrogen versus CO/H_2 mixtures), (ii) the substrate temperature (with a different behaviour below and above ~125 K), and (iii) the Pd surface structure (Pd particles versus single crystals). Six different "coadsorption scenarios" were identified (not shown here), which could be explained considering that (i) H does not diffuse subsurface below ~125 K on Pd(1 1 1) due to the 0.5 eV activation barrier, (ii) that adsorbed H destabilizes on-top CO on Pd(1 1 1), (iii) that Pd-hydride phases (composition ranging from ~$PdH_{0.3}$ to ~$PdH_{0.8}$ [93]) are more easily formed for Pd nanoparticles, and (iv) that the small volume of Pd nanoparticles "overrules" structure effects in CO–H coadsorption (finite size effects[7]). These results made quite clear that UHV experiments can hardly be extrapolated to the reaction conditions of CO

[5] Noble metal nanoparticles of industrial catalysts often exhibit a higher height/diameter ratio, i.e. they rather approach hemispheres, and the contribution of (1 0 0) facets may be higher.

[6] "Intensity borrowing" refers to an effect where coupling between oscillators results in an apparent transfer of intensity from e.g. a low- to high-frequency oscillator [76,92]. As a result, the spectral intensities no longer correlate with the number/concentration of oscillators leading e.g. to an apparent enhancement of a high-frequency absorbance.

[7] For example, hydride decomposition is very different for Pd nanoparticles and Pd single crystals when the Pd surfaces are covered by CO. For CO-covered Pd nanoparticles, hydrogen desorption resulting from hydride decomposition occurred at 245 K, whereas for CO-covered Pd single crystals hydrogen desorption resulting from hydride decomposition was observed at ~370 K; for details see [93].

hydrogenation and that only *in situ* spectroscopy can identify the relevant surface species.

SFG spectra of CO–H interaction were thus also acquired under high-pressure/high-temperature conditions, when a dynamic equilibrium between gas phase and surface species was established [93,97]. Fig. 4c shows an SFG spectrum acquired on Pd–Al_2O_3 at 500 K, in the presence of 100 mbar CO and 1 bar hydrogen. Two resonances were observed, at 1955 cm^{-1} originating from bridge-bonded CO (at steps/edges and (1 1 1) terraces), and at 2055 cm^{-1} originating from on-top CO. A weak shoulder at ~1930 cm^{-1} (this band can be better discerned by fitting) may originate from bridge or hollow bonded CO (the exact assignment of CO resonances to either bridge or hollow bonded CO is still a somewhat open question [99,100]).

The *in situ* spectrum reveals two characteristics of the high-pressure/high temperature reaction. First, the spectrum is characteristic for a CO coverage around 0.5 ML. Under static UHV conditions no dissociative hydrogen adsorption occurred for CO coverages above 0.2–0.3 ML [97], in accordance with the ~2.5 eV activation barrier suggested by DFT for hydrogen adsorption on CO-covered Pd(1 1 1) [86]. Under static UHV conditions, such high CO coverages thus prevent hydrogen adsorption. Furthermore, recent STM observations of H/Pd(1 1 1) suggest that dissociative hydrogen adsorption requires at least three neighboring empty Pd sites [101] which are difficult to find at such high CO coverages and render hydrogen adsorption even more unlikely. However, a static (UHV) picture is not appropriate for reaction conditions. Under the dynamic conditions of a high-pressure reaction even the unlikely event of hydrogen adsorption has a non-zero probability due the adsorption/desorption equilibrium of CO and the high hydrogen impingement rate (which is about 40 times higher than that of CO and on the order of 10^8/Pd surface atoms·sec). Isotope exchange experiments indicated that even at 200 K a CO layer was exchanged within minutes [49]. Even if only a negligible number of free adsorption sites are present resulting from thermal fluctuations on the CO covered surface (e.g. one site per 10^6 Pd atoms), the high H_2 impingement rate allows for a non-negligible hydrogen adsorption.

Second, the high-pressure spectrum in Fig. 4c was different from corresponding UHV spectra for $\theta_{CO} \sim 0.5$. At high temperature a bridging species at 1955 cm^{-1} was typically not accompanied by an on-top feature around 2055 cm^{-1}. Such a low-frequency on-top CO species does not occur under UHV and points to a possible surface roughening under reaction conditions. However, the high-pressure adsorbate phase was not induced by hydrogen because corresponding spectra of (pure) CO were nearly identical [93]. In any case, post-reaction CO-SFG did not indicate any strong surface reconstruction or modified spectrum (such as a significantly increased intensity of on-top CO which would be characteristic for rougher surfaces [50,87]). This indicates that the CO-induced roughening must either be reversible or rather moderate, if present at all. Alternatively, the enhanced on-top CO species at mbar pressure could also originate from a partially disordered CO phase on the particle facets which may facilitate CO–H interaction. According to DFT calculations favouring the CO + H reaction over a single metal atom [102] the on-top CO species should react with bridge/hollow bonded H to produce CHO (formyl).

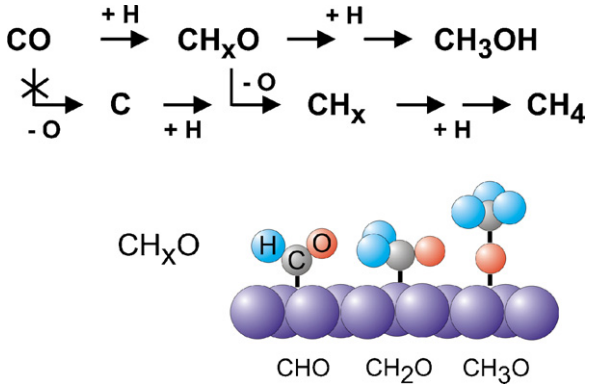

Fig. 5. Schematic illustration of potential CO hydrogenation routes on Pd catalysts.

Fig. 5 shows the suggested reaction mechanism which is further supported by corresponding HP-XPS investigations (not shown here) [103]. According to HP-XPS of CO interaction with smooth and rough Pd surfaces at pressures up to 1 mbar, CO dissociation does not occur on Pd [27,104]. SFG did also not find indications for CO dissociation, even after extended high-pressure CO exposure of Pd nanoparticles (such as deactivation of Pd particles by surface carbon species). A non-dissociative reaction pathway should then yield methanol as only reaction product but Pd catalysts also produce significant amounts of methane [105–107]. This suggests that there must be a second route, i.e. the direct hydrogenation of CO ($CO + xH \leftrightarrow CH_xO$), followed by C–O bond scission ($CH_xO \leftrightarrow CH_x + O$) and hydrogenation to methane (or further dehydrogenation of CH_x), as illustrated in Fig. 5.[8] In fact, HP-XPS spectra acquired in the presence of CO/H_2 mixtures indicated CH_x species that originated from C–O bond scission within CH_xO (the most likely precursor is CH_2O, as discussed below). As indicated by a comparison of ion-bombarded and (smooth) Pd(1 1 1), the first step of this route (CH_xO formation) seems to be facilitated by surface defects, whereas the second step (CH_xO decomposition to CH_x) is fast even on both surfaces [104,108]).

The probability of C–O bond scission within CO or CH_xO is probably related to the adsorption geometry of these species. While CO adsorbs perpendicular on Pd(1 1 1), the C–O bond within CHO and CH_2O species is tilted with respect to the Pd substrate (cf. Fig. 7) [109]. The tilted arrangement may allow for a better overlap between the CH_xO orbitals and the metal valence electron density, thus weakening the C–O bond. Further experiments and calculations are certainly required to fully understand the hydrogenation process. In particular, to elucidate the effect of promoters such as Li or Ca remains a challenge. Li- or Ca-promoted Pd catalysts produce nearly 100% methanol [110] suggesting that on these catalysts C–O bond scission does not occur.

[8] Formation of dimethyl ether as another product also suggests both routes occurring simultaneously.

Summarizing, it is evident that the equilibrium conditions of a high-pressure reaction led to adsorbate arrangements that could not be reproduced under static UHV conditions. One should also note that the SFG spectrum at 1.1 bar on Pd–Al_2O_3 (Fig. 4c) is very similar to IR spectra reported by Hicks and Bell [111] for 5% Pd–silica at ∼10 bar, indicating that a well-defined model catalyst is able to mimic a technological catalyst quite well. As mentioned, β-Pd-hydride is not stable under the applied reaction conditions. However, there is a considerable amount of dissolved hydrogen (as detected by post-reaction H_2-TPD) and its involvement in the catalytic reaction cannot be ruled out. The exact nature and amount of dissolved hydrogen could, however, not be determined under high-pressure reaction conditions.

3.2. Partial methanol oxidation on Pd–Al_2O_3 and Pd(1 1 1)

Methanol decomposition and oxidation on noble metals are prototypical reactions of surface science, modelling the interaction of catalysts with alcohols or small organic molecules. A large number of UHV studies were reported (e.g. [72,108,109,112–124]). However, UHV studies that are frequently performed by adsorbing molecules at low temperature and by spectroscopically monitoring chemical changes upon annealing are not necessarily representative for a technical catalytic reaction. For instance, CH_3OH desorbs (multilayer at 140 K, monolayer at 175 K) before it reacts, whereas for the high-pressure/high temperature reaction the surface species are in equilibrium with the gas phase.

3.2.1. Methanol oxidation on Pd(1 1 1)

Fig. 6 summarizes results of a combined PM-IRAS/GC elevated pressure study of methanol decomposition and oxidation on Pd(1 1 1) [72,74,125,126], displaying (p − s) surface spectra, (p + s) gas phase spectra (which are basically identical to s-spectra), and an analysis of kinetic turnover by gas chromatography and by analysis of the (p + s) PM-IRAS spectra.[9] In the absence of oxygen, i.e. at 5 mbar CH_3OH at 300 K, all dehydrogenation products of methanol were observed: methoxy CH_3O (minute amounts around 2900 cm^{-1}; not shown; cf. Fig. 3a in [74]), formaldehyde CH_2O (ρCH_2 of formaldehyde in two different adsorption geometries at 1305 and 1255 cm^{-1} [127]),[10] formyl CHO (CH bending or ν_{CO} at 1200 cm^{-1} [129]), and adsorbed CO (ν_{CO} at ∼1840 cm^{-1}, typical of ∼0.3 ML coverage). Concerning the dehydrogenation process (illustrated in Fig. 7), there is general agreement in the literature (apart from smaller variations of the reported transition temperatures and of the thermal stability of the different species). Apart from these adsorbate species, carbonaceous overlayers (CH_x) in excess of 1 ML were observed by *in situ* [108] and post-reaction XPS [74], which must result from C–O bond scission. According to combined SFG/HP-XPS investigations of methanol decomposition, CH_x is most likely elemental carbon [108]. Hence, the surface was self-poisoned by CO, CHO, CH_2O, and CH_x and methanol decomposition does thus not work (on a macroscopic scale) under these conditions. No activity for methanol decomposition was detected by GC analysis (Fig. 6c) and also corresponding PM-IRAS gas phase spectra only detected the reactant CH_3OH (Fig. 6b).

In order to start the reaction, 5 mbar oxygen were added and the temperature was increased. Up to 350 K all surface species remained almost unchanged, with no catalytic activity. The onset of catalytic activity was observed at 400 K, with CH_2O, CO_2 and H_2O identified as gas phase products by GC and PM-IRAS (p + s) spectra (Fig. 6c and d). The CH_3OH conversion after 3 h at 400 K was ∼84%, yielding a turnover frequency of seven methanol molecules converted per Pd surface atom and second (initial turnover frequency of 15/site sec after 90 min of reaction), and with a product distribution of ca. 10% CH_2O and 25% CO_2.

For the Pd surface at 400 K, PM-IRAS detected CO as only surface species whereas formaldehyde and formyl had disappeared (Fig. 6a). Apparently, at 400 K CH_2O and CHO were reacted away, either by dehydrogenation to CO and/or by desorption. The reduced amount of CH_2O and CHO (and CH_x; see below) under reaction conditions generated more free surface sites and led to a higher CO surface coverage, indicated by the shift of the CO peak to ∼1890 cm^{-1} (typical of ∼0.4 ML CO) (Fig. 6a).

From these observations one can conclude that methanol oxidation proceeds via dehydrogenation to CH_2O, which either desorbs or is further dehydrogenated to CO, which is subsequently oxidized to CO_2 (Fig. 7). During the various dehydrogenation steps, reaction of hydrogen and oxygen produces water. Unfortunately, the surface concentration of CH_2O (and CHO) is below the detection limit under reactive conditions. Hollow bonded CO was identified by PM-IRAS but it can currently not be excluded that these molecules are spectators and that CO_2 formation rather proceeds via short-lived weaker bonded CO (isotope experiments have to answer this question in the future).

Under reaction conditions at 400 K, *in situ* HP-XPS and post-reaction XPS detected about 0.4 monolayers of CH_x species [74]. C–O bond scission could principally occur within methoxy, formaldehyde and/or formyl, followed by further dehydrogenation (while CO dissociation was not observed [104]). The very weak peak around 1720 cm^{-1} (Fig. 6a) can be assigned to ν(C–O) of formaldehyde [130] or to ν(C–O) of a formyl species [129]. Its weak intensity suggests that the C–O bond is oriented (nearly) parallel to the surface (c.f. Fig. 7) and CH_2O therefore seems the most likely precursor for C–O bond cleavage, due to the orientation of the C–O parallel to the Pd surface (whereas for CO the C–O bond is perpendicular to the Pd surface, probably explaining the non-occurrence of CO dissociation).

[9] Fig. 6d was obtained by integration of the gas phase peaks in the (p + s) PM-IRAS spectra. The plotted lines only *qualitatively* show the disappearance/evolution of the different components because the peak areas were not calibrated.

[10] According to [127] formaldehyde is adsorbed in bridging and chelating geometry. A contribution of formate [128] cannot be excluded but will not be considered here.

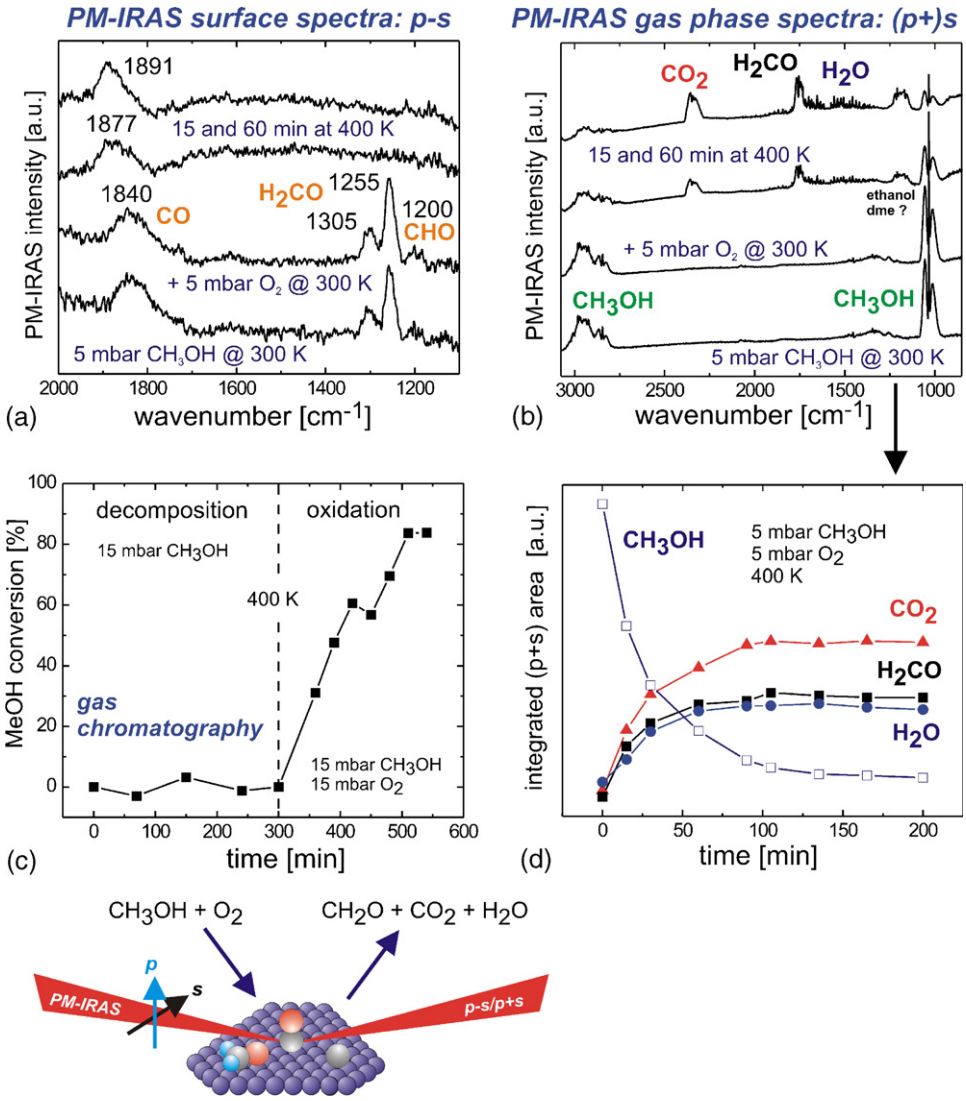

Fig. 6. *In situ* PM-IRAS surface (a) and gas phase (b) spectra characterizing elevated pressure CH_3OH decomposition and oxidation on Pd(1 1 1). Methanol conversion was monitored via gas chromatography (c) and via PM-IRAS (d); adapted from [74] with permission. Copyright (2005) American Chemical Society.

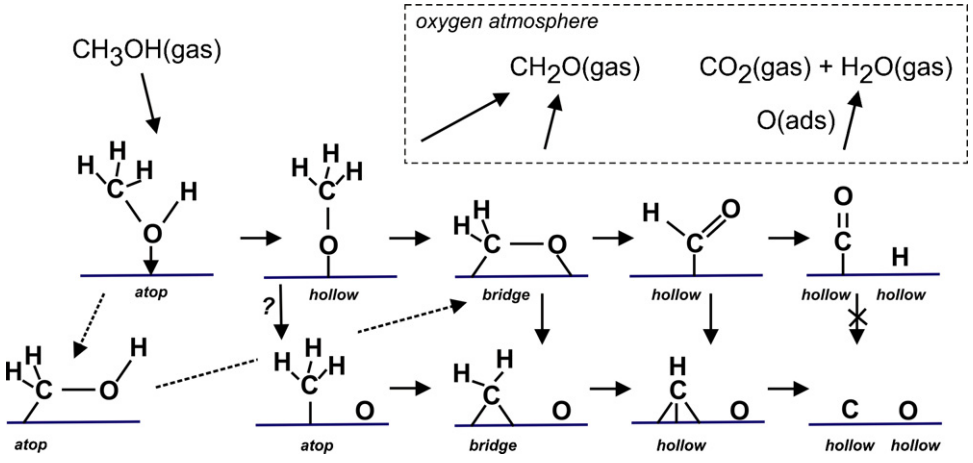

Fig. 7. Suggested mechanism of CH_3OH decomposition and oxidation on Pd catalysts.

As mentioned, CH_x is most likely elemental carbon, which adsorbs at hollow sites [108,131]. This may induce a lowering of activity by reducing the Pd surface area but the carbon species may also influence the reaction selectivity. In fact, combined time-dependent XPS and PM-IRAS spectroscopy have shown that the evolution of CH_x species and of adsorbed CH_2O is temporally correlated [74]. On a clean Pd surface, CH_3OH decomposed to CO whereas on a carbon-poisoned surface the amount of adsorbed CO decreased and more and more adsorbed CH_2O was observed. An influence of the CH_x species on the reaction selectivity is thus very likely.

This can be rationalized considering that carbon adsorbed on threefold hollow sites hinders CH_2O dehydrogenation to CHO and CO by blocking the required (hollow) sites and CH_x may thus favour CH_2O formation. Fig. 7 shows a proposed reaction mechanism based on the experimental findings and on DFT calculations of Neurock, Mavrikakis, and others (see references cited in [109,124,132]). On a clean Pd(1 1 1) surface, CH_3OH adsorbs at top sites and is dehydrogenated via CH_3O (on threefold hollow sites), and via CH_2O (on bridge sites), and via CHO (on hollow sites) to give CO adsorbed on hollow sites. Apart from a possible effect of carbon on CH_2O decomposition, CH_x species occupying hollow sites may also hinder CH_3O formation, and CH_3OH may instead react to give hydroxymethyl (CH_2OH), which binds to free on-top sites. CH_2OH is then dehydrogenated to CH_2O, and, as mentioned, further dehydrogenation to CHO and CO is presumably hindered, because the required hollow sites are occupied by CH_x. Accordingly, a clean surface would preferentially produce CO_2, whereas a partly CH_x-deactivated surface would also produce CH_2O. However, CH_2OH could not be identified spectroscopically and a conclusive proof is thus difficult to achieve. Nevertheless, this model is supported by the observation that at reaction temperatures of 500 K or higher, when the CH_x concentration is much smaller (according to XPS), only CO_2 and water were observed as products in PM-IRAS (p + s) spectra (not shown).

One also has to take into account that GC and PM-IRAS detected small amounts of ethanol and dimethyl ether. Because ethanol can be produced from the reaction of CH_2OH with CH_3, and dimethyl ether from methoxy (CH_3O) and CH_3, both products indicate an involvement of CH_3 groups. Consequently, a dehydration pathway ($2CH_3OH \rightarrow CH_3O + CH_3 + H_2O$) [119] and C–O bond scission within CH_3OH or CH_3O (although energetically unfavourable [124]) should not be neglected, because both produce the required methyl groups. It is emphasized that a complete understanding has not yet been obtained, consistent with the large number of potential surface species (CH_3OH, CH_3O, CH_2OH, CH_2O, CHO, CO, H, CH_x, O, CO_2, H_2O, and possibly formate). Apart from geometric effects, CH_x species may also change the electronic structure of neighbouring palladium sites [133]. Detailed GC investigations of selectivity combined with *in situ* XPS measurements of reacting surfaces will be required to assess this model critically.

A final key question concerns the state of the Pd(1 1 1) surface during the oxidation reaction at mbar pressure at 400 K (or higher). Surface oxides of Pd (Pd_5O_4 overlayer [134–136]) and of other metals [137–139] that may form during a high-pressure reaction have recently raised much attention and may contribute to a reaction by supplying oxygen. It has also been suggested that surface oxides may even constitute the active phase [33]. For high temperature oxidation reactions on Pd, such as methane combustion, Pd-oxide phases (e.g. PdO) are more or less accepted as active components ([140] and references cited therein). However, for low-temperature reactions such as CO oxidation (which is part of methanol oxidation) the metallic phase is typically considered to be more active (a detailed discussion will follow below). For our study on Pd(1 1 1), *in situ* HP-XPS and post-reaction XPS in the Pd 3d and O 1s regions did not indicate any surface oxidation [74]. Furthermore, the CO species observed during the oxidation reaction by PM-IRAS were characteristic of adsorption on metallic Pd. Consequently, the oxidation of the Pd(1 1 1) surface, if present at all, must be minor.

3.2.2. Methanol oxidation on Pd–Al_2O_3

The same type of experiments were also performed for Pd nanoparticles (mean diameter 6 nm) supported on Al_2O_3/NiAl(1 1 0), with the main results summarized in Fig. 8 [125,126,141,142]. Similar to Pd(1 1 1), the onset of catalytic activity was at 400 K (Fig. 8a) and bridge and on-top bonded CO were the only surface species observed by SFG (Fig. 8b). The assignment of the CO bands was based on previous studies of CO adsorption (cf. Section 3.1) and for an explanation of SFG lineshapes and peak positions we refer to [83]. After the reaction, about 0.5 ML CH_x were detected. However, for identical reaction conditions there was a marked difference between Pd(1 1 1) and Pd–Al_2O_3. Whereas Pd(1 1 1) remained metallic through the reaction, post-reaction XPS indicated a significant oxidation of Pd particles during the high-pressure reaction (Fig. 8c). The ~0.6 eV binding energy shift observed by XPS indicates an oxidation state in between Pd and PdO (the binding energy shift for PdO would be 1.5 eV [140]), denoted here as PdO_x. Nevertheless, the observed vibrational frequencies of adsorbed CO were characteristic of metallic Pd. Titration of the particle surface after the reaction by using CO as probe molecule revealed that about 50% of the particle surface was oxidized. Such partially oxidized Pd/PdO_x nanoparticles were investigated in detail by Schalow et al. [143].

Now it is of course interesting to discuss the specific activity of Pd and PdO_x for methanol oxidation (and thus CO oxidation). When the Pd particles were strongly oxidized, e.g. by preoxidation around 450 K or after reaction under oxygen-rich conditions, the catalysts were quite inactive for CH_3OH oxidation. This implies that the oxide phases are less active than metallic Pd in CH_3OH (and CO) oxidation. Studies of CO oxidation on partially oxidized Pd/PdO_x nanoparticles and on various PdO_x surfaces using molecular beams, TPD, XPS and TEM, were reported in [144,145]. These investigations showed that the activity of Pd-oxide phases (such as Pd_5O_4) was at least four to five times lower than the activity of chemisorbed oxygen on metallic Pd. When PdO phases were produced by stronger oxidation [145], the activity for CO

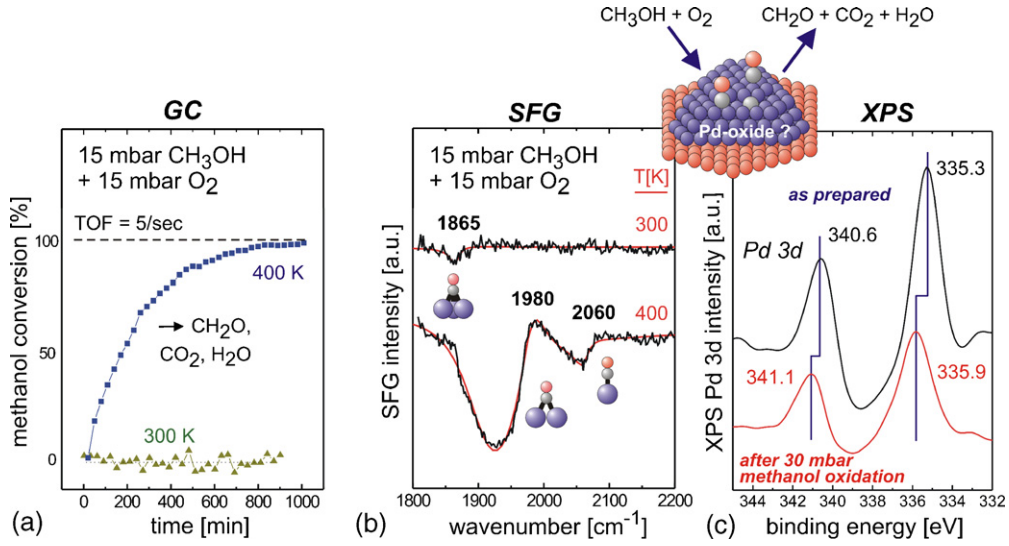

Fig. 8. Methanol oxidation on Pd–Al_2O_3/NiAl(1 1 0) (mean particle diameter 6 nm): (a) CH_3OH conversion vs. reaction time, monitored by gas chromatography, and (b) corresponding *in situ* SFG spectra. (c) Pd 3d XPS spectra acquired before and after high-pressure methanol oxidation indicate a partial oxidation of the Pd particles during the reaction. Because the particles were covered by CO after the reaction, the clean sample was also exposed to CO, responsible for the shift from 334.9 to 335.3 eV; adapted from [126,141].

oxidation vanished and a reduction of PdO by CO could only be achieved in 10 mbar CO at 523 K.

3.3. More complex catalysts and more complex reactions

Al_2O_3 is a widely used, rather inert support material. A number of other well-defined crystalline and atomically flat oxide films has recently been developed (for a review see [146]) that can also be used as model supports, including SiO_2, FeO, Fe_2O_3, Fe_3O_4, V_2O_3, V_2O_5, Nb_2O_5, TiO_2, MgO, etc. These oxides have in part been utilized as supports for Pd, Pt, Rh, Ag, Au, bimetallic, etc., nanoparticles [37,38]. One has to realize, however, that when oxides exist in various metal oxidation states and when they are less inert than Al_2O_3, the complexity of the model studies strongly increases.

As an example, we discuss CO adsorption on Pd nanoparticles (mean diameter 3.5 nm) supported on Nb_2O_5/Cu_3Au(1 0 0) [147]. The preparation and structure of thin Nb_2O_5 films were investigated by the groups of Niehus and Freund and have been described in detail in [148,149]. Very briefly, the Nb_2O_5 oxide film is ~0.4 nm thick and grows two-dimensionally, forming terraces ~100 nm wide. On top of the Cu_3Au substrate there is a close packed O layer on which Nb cations in oxidation state close to 5^+ occupy hollow sites and form a $(\sqrt{3} \times \sqrt{3})R30^\circ$ structure (Nb coverage 2/3 ML). There is another oxygen layer on top of the Nb lattice, leading to a O–Nb–O–Cu_3Au stacking. It is worth noting that this oxide surface structure does not coincide with any truncation of a bulk Nb-oxide structure.

In contrast to Pd–Al_2O_3, the Pd–Nb_2O_5 model system undergoes strong structural changes when annealed above 300 K. Fig. 9 shows TPD and SFG spectra examining the effect of annealing via CO adsorption. CO-TPD (Fig. 9a) indicated that the first spectrum was characteristic of CO desorption from Pd particles whereas repeated TPD spectra indicated that 50% of the CO adsorption capacity had been lost and that the desorption temperatures (which are characteristic for the CO adsorption energy on the various sites) had changed. In order to determine at which temperature these changes occurred, SFG (CO saturation) spectra were acquired at 110 K after annealing a "fresh" model catalyst to the indicated temperatures (Fig. 9b). Upon heating the Pd–Nb_2O_5 model catalyst to 300 K and higher the spectra changed, i.e. the SFG signal intensities and the lineshape were altered (a quantitative analysis of the spectra is shown in Fig. 9c). The lineshape change results from a change in the SFG nonresonant background and indicates a modification of the electronic structure of the surface [83]. Simple Pd particle sintering or (partial) encapsulation of Pd particles by the niobia support (that would also lead to a loss of CO adsorption capacity) cannot explain the observed lineshape change and the formation of "mixed Pd–NbO_x" sites upon annealing to >300 K was made responsible to cause the observed effect. One should note that this is a thermal effect, i.e. it also occurs in the absence of CO (CO just acts as probe molecule here). Similar changes were observed for Co-Nb_2O_5 [150]. Unfortunately, this "instability" somewhat limits the usefulness of this model system, at least until a stabilization/activation procedure has been developed. Nevertheless, mixed metal–NbO_x compounds" have been proposed as key components of active Fischer–Tropsch catalysts [151].

Model systems can also be applied to more complex reactions. Pd–Al_2O_3 model catalyst with mean particle diameters in the range of 2–8 nm were used to examine size effects in selective 1,3-butadiene hydrogenation [152,153]. Butadiene hydrogenation gives four products (1-butene, *trans*-2-butene, *cis*-2-butene, and n-butane) with 1-butene typically being the desired product. Although selectivity is the critical issue for this reaction, here we focus on the initial catalytic activity (reaction time ~60 min). Fig. 10a displays the initial

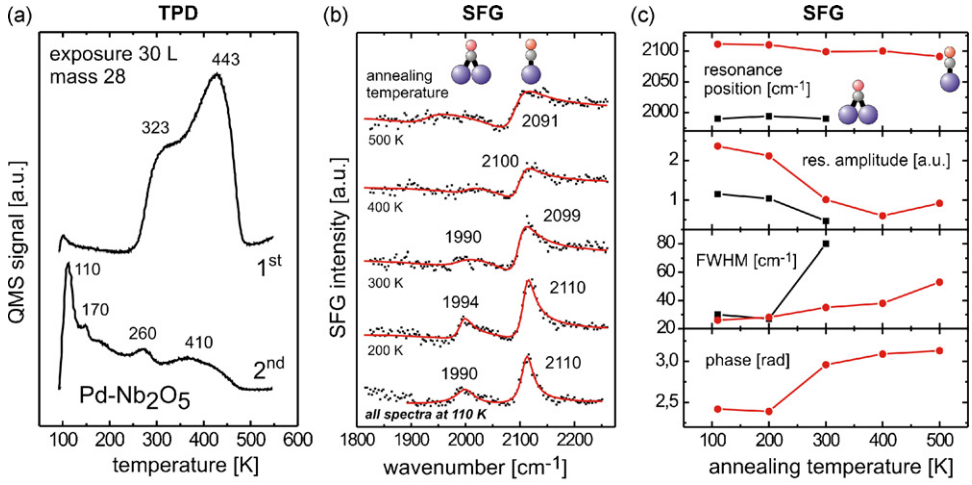

Fig. 9. (a) TPD spectra of CO adsorbed on 3.5 nm Pd particles supported on $Nb_2O_5/Cu_3Au(1\,0\,0)$ (exposure 30 L CO at 100 K) indicating a 50% loss of CO adsorption capacity upon annealing (as well as changes in the adsorption states). (b) SFG spectra acquired in 10^{-6} mbar CO at 110 K, after annealing the model catalysts to the indicated temperatures. The values obtained for the peak position, resonant amplitude, peak width (FWHM) and phase ϕ of the spectra are plotted in (c) for on-top and bridge-bonded CO. Metal–support interaction upon annealing to $\geq$300 K leads to the formation of a mixed "Pd–NbOx" phase, responsible for the irreversible loss of CO adsorption capacity; adapted from [147] with permission from Elsevier.

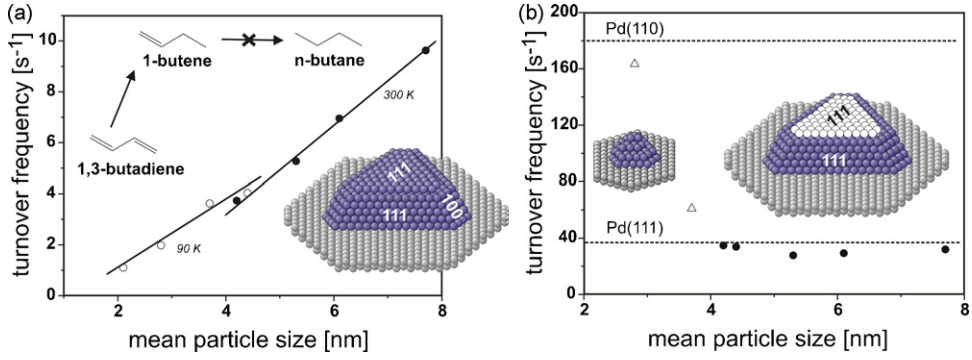

Fig. 10. Selective 1,3-butadiene hydrogenation on $Pd–Al_2O_3/NiAl(1\,1\,0)$ at 373 K: turnover frequency (TOF) for the different $Pd–Al_2O_3$ catalysts as a function of mean particle diameter, normalized by the total number of Pd surface atoms (a), and normalized by the number of Pd atoms on incomplete (1 1 1) facets (b), using a truncated cubo-octahedron as realistic structural model (shown as inset; incomplete layers on side facets are not displayed for graphical reasons). TOF values for Pd(1 1 1) and Pd(1 1 0) single crystals under identical reaction conditions are shown as dashed lines. Reaction conditions: 5 mbar 1,3-butadiene; 10 mbar H_2; Ar added up to 1 bar; adapted from [152] with permission from The Royal Society of Chemistry.

activity, presented as turnover frequency, as a function of mean Pd particle diameter. For this plot, the total number of Pd surface atoms was used for rate normalization, yielding a clear particle size dependence, in agreement with earlier reports [154].

However, why should all Pd surface atoms be equally active? Single crystal studies have indicated a five-fold activity difference between Pd(1 1 0) and Pd(1 1 1) [155,156]. Therefore, we have tried to correlate the absolute activity of a catalyst (i.e. the total number of butadiene molecules converted) with the total number of specific surfaces atoms/sites of a catalyst (such as Pd atoms at (1 1 1) facets, (1 0 0) facets, step and edge sites, interface sites, etc). A good correlation was only found for incomplete (1 1 1) surface facets [153]. An incomplete (1 1 1) facet (with atoms missing around the perimeter of the uppermost layer) is shown in white in the model in Fig. 10b (such incomplete surface facets were e.g. observed by HRTEM [47] and STM [45]). Fig. 10b also shows the particle size dependence of the reaction rate (filled dots), this time using the number of Pd atoms in incomplete (1 1 1) facets for rate normalization. The TOF is now clearly particle size independent, at least for Pd particles >4 nm.[11] This indicates that the Pd atoms in the (1 1 1) facets are the active sites. To support this claim we have measured the absolute rate of 1,3-butadiene hydrogenation on a Pd(1 1 1) single crystal surface [156]. The value of 38 s^{-1} coincides very well with the specific activity of the Pd nanoparticles suggesting that the (1 1 1) facets are in fact the active ones.

In situ vibrational spectroscopy investigations were not successful for this reaction yet [157], which may be due to the small surface concentration of the species adsorbed at 373 K and/or to the flat orientation of the unsaturated molecules with

[11] Pd particles below 3 nm diameter do not have well-developed facets so that the normalization is not really meaningful (open triangles in Fig. 10b).

the C–H bonds nearly parallel to the Pd surface. Nevertheless, this study is an example of how the ''materials gap'' between heterogeneous catalysis on metal nanoparticles and surface science on single crystals can be bridged on a *quantitative* basis, by showing that here Pd particles larger than 4 nm behave very similar to Pd(1 1 1).

4. Synopsis

A number of case studies were presented to illustrate how ambient pressure spectroscopy on planar nanoparticle model catalysts can help to understand fundamental processes of heterogeneous catalysis. Supported Pd nanoparticles behave different from Pd single crystals, as discussed for CO adsorption, H adsorption/absorption and CO–H coadsorption. These differences are often due to structure effects, for instance the presence of edge and step sites on nanoparticles (and these sites can typically not be fully modelled even with stepped single crystals). However, apart from structure effects, the mere ''finite size'' (or limited volume) of Pd nanoparticles may govern their interaction with gas molecules, particularly with hydrogen. No ''high-pressure species'' were observed, but the site populations under high-pressure reaction conditions may be different from those observed under UHV. Ambient pressure studies of methanol partial oxidation revealed that C–O bond scission, which is of minor importance under UHV, may strongly influence the reaction under technically more relevant conditions. Formaldehyde may be the precursor for surface CH_x species that, in turn, favourably affect the selectivity towards CH_2O. These investigations also indicated that Pd particles were more easily oxidized under reaction conditions than Pd(1 1 1). Nevertheless, metallic Pd was more active than PdO_x phases.

Recent progress in the development of more complex model catalysts and their application to technically more relevant reactions, which require controlling selectivity, let model catalysis slowly approach the interesting topics of applied catalysis, but also its problems. To successfully continue the development of model catalysis is the challenge of the years to come.

Acknowledgements

Most of the results presented were obtained at the Fritz Haber Institute (Berlin, Germany). I am very grateful to previous and present coworkers and colleagues whose names appear in the list of references. In particular, I want to thank T. Dellwig, H. Unterhalt, L. Hu, P. Galletto, M. Morkel, O. Rodriguez de la Fuente, M. Borasio, F. Höbel, B. Kell, J. Silvestre-Albero, and A. Bandara, and I am very much indebted to H.-J. Freund for continuous support (all Fritz Haber Institute, Berlin). Long-time collaborations with V.I. Bukhtiyarov (Boreskov Institute of Catalysis), K. Hayek (University Innsbruck), R. Schlögl (Fritz Haber Institute, Berlin) and G.A. Somorjai (University of California at Berkeley) are gratefully acknowledged. The STM images in Fig. 1b are courtesy of M. Heemeier and M. Bäumer.

References

[1] G.A. Somorjai, Langmuir 7 (1991) 3176.
[2] G.A. Somorjai, Chem. Rev. 96 (1996) 1223.
[3] D.W. Goodman, Chem. Rev. 95 (1995) 523.
[4] G.A. Somorjai, G. Rupprechter, J. Chem. Educ. 75 (1998) 161.
[5] M.E. Levin, K.J. Williams, M. Salmeron, A.T. Bell, G.A. Somorjai, Surf. Sci. 195 (1988) 2807.
[6] K. Hayek, M. Fuchs, B. Klötzer, W. Reichl, G. Rupprechter, Top. Catal. 13 (2000) 55.
[7] H.-J. Freund, Angew. Chem. Int. Ed. Engl. 36 (1997) 452.
[8] C.T. Campbell, Surf. Sci. Rep. 27 (1997) 1.
[9] C.R. Henry, Surf. Sci. Rep. 31 (1998) 235.
[10] H.-J. Freund, M. Bäumer, H. Kuhlenbeck, Adv. Catal. 45 (2000) 412.
[11] D. Goodman, J. Catal. 216 (2003) 213.
[12] K. Hayek, J. Mol. Catal. 51 (1989) 347.
[13] C.R. Henry, C. Chapon, C. Goyhenex, R. Monot, Surf. Sci. 272 (1992) 283.
[14] G. Rupprechter, G. Seeber, K. Hayek, H. Hofmeister, Phys. Stat Sol. (a) 146 (1994) 449.
[15] P.L.J. Gunter, J.W.H. Niemantsverdriet, F.H. Ribeiro, G.A. Somorjai, Catal. Rev.-Sci. Eng. 39 (1997) 77.
[16] H.-J. Freund, Surf. Sci. 500 (2002) 271.
[17] G. Rupprechter, Annu. Rep. Progr. Chem, Sect. C 100 (2004) 237.
[18] J. Libuda, H.-J. Freund, J. Phys. Chem. B 106 (2002) 4901.
[19] S.M. Davis, F. Zaera, G.A. Somorjai, J. Am. Chem. Soc. 104 (1982) 7453.
[20] R.A. Campbell, D.W. Goodman, Rev. Sci. Instrum. 63 (1992) 172.
[21] G.A. Somorjai, Z. Phys. Chem. 197 (1996) 1.
[22] G.A. Somorjai, G. Rupprechter, J. Phys. Chem. B 103 (1999) 1623.
[23] W. Reichl, G. Rosina, G. Rupprechter, C. Zimmermann, K. Hayek, Rev. Sci. Instrum. 71 (2000) 1495.
[24] G. Rupprechter, T. Dellwig, H. Unterhalt, H.-J. Freund, Top. Catal. 15 (2001) 19.
[25] D. Ogletree, H. Bluhm, G. Lebedev, C. Fadley, Z. Hussain, M. Salmeron, Rev. Sci. Instrum. 73 (2002) 3872.
[26] H. Bluhm, M. Hävecker, E. Kleimenov, A. Knop-Gericke, A. Liskowski, R. Schlögl, D.S. Su, Top. Catal. 23 (2003) 99.
[27] V.V. Kaichev, I.P. Prosvirin, V.I. Bukhtiyarov, H. Unterhalt, G. Rupprechter, H.-J. Freund, J. Phys. Chem. B. 107 (2003) 3522.
[28] V.I. Bukhtiyarov, V.V. Kaichev, I.P. Prosvirin, Top. Catal. 32 (2005) 3.
[29] J. Pantförder, S. Pöllmann, J.F. Zhu, D. Borgmann, R. Denecke, H.-P. Steinrück, Rev. Sci. Instrum. 76 (2005) 014102.
[30] J.A. Jensen, K.B. Rider, M. Salmeron, G.A. Somorjai, Phys. Rev. Lett. 80 (1998) 1228.
[31] E. Lægsgaard, L. Österlund, P. Thostrup, P.B. Rasmussen, I. Stensgaard, F. Besenbacher, Rev. Sci. Instrum. 72 (2001) 3537.
[32] A. Kolmakov, D.W. Goodman, Rev. Sci. Instrum. 74 (2003) 2444.
[33] B.L.M. Hendriksen, J.W.M. Frenken, Phys. Rev. Lett. 89 (2002) 046101.
[34] M.A. Banares, Catal. Today 100 (2005) 71.
[35] J. Libuda, F. Winkelmann, M. Bäumer, H.-J. Freund, T. Bertrams, H. Neddermeyer, K. Müller, Surf. Sci. 318 (1994) 61.
[36] M. Bäumer, L. Libuda, A. Sandell, H.-J. Freund, G. Graw, T. Bertrams, H. Neddermeyer, Ber. Bunsenges. Phys. Chem. 99 (1995) 1381.
[37] M. Bäumer, H.-J. Freund, Prog. Surf. Sci. 61 (1999) 127.
[38] H.-J. Freund, M. Bäumer, J. Libuda, T. Risse, G. Rupprechter, S. Shaikhutdinov, J. Catal. 216 (2003) 223.
[39] K.H. Hansen, T. Worren, S. Stempel, E. Lægsgaard, M. Bäumer, H.-J. Freund, F. Besenbacher, I. Stensgaard, Phys. Rev. Lett. 83 (1999) 4120.
[40] K. Hojrup-Hansen, T. Worren, E. Lægsgaard, F. Besenbacher, I. Stensgaard, Phys. Rev. Lett. 86 (2001) 4120.
[41] A. Stierle, F. Renner, R. Streitel, H. Dosch, W. Drube, B.C. Cowie, Science 303 (2004) 1652.
[42] G. Kresse, M. Schmid, E. Napetschnig, M. Shishkin, L. Köhler, P. Varga, Science 308 (2005) 1440.

[43] M. Schmid, M. Shishkin, G. Kresse, E. Napetschnig, P. Varga, M. Kulawik, N. Nilius, H.-P. Rust, H.-J. Freund, Phys. Rev. Lett. 124 (2006) 046101.
[44] M. Kulawik, N. Nilius, H.-P. Rust, H.-J. Freund, Phys. Rev. Lett. 91 (2003) 256101.
[45] M. Frank, M. Bäumer, Phys. Chem. Chem. Phys. 2 (2000) 3723.
[46] M. Heemeier, S. Stempel, S. Shaikhutdinov, J. Libuda, M. Bäumer, R.J. Oldman, S.D. Jackson, H.-J. Freund, Surf. Sci. 523 (2003) 103.
[47] G. Rupprechter, Phys. Chem. Chem. Phys. 3 (2001) 4621.
[48] S. Shaikhutdinov, M. Heemeier, J. Hoffmann, I. Meusel, B. Richter, M. Bäumer, H. Kuhlenbeck, J. Libuda, H.-J. Freund, R. Oldman, S.D. Jackson, C. Konvicka, M. Schmid, P. Varga, Surf. Sci. 501 (2002) 270.
[49] H. Unterhalt, G. Rupprechter, H.-J. Freund, J. Phys. Chem. B. 106 (2002) 356.
[50] G. Rupprechter, H. Unterhalt, M. Morkel, P. Galletto, L. Hu, H.-J. Freund, Surf. Sci. 502–503 (2002) 109.
[51] P. Thüne, J. Loos, A. de Jong, P. Lemstra, J.W. Niemantsverdriet, Top. Catal. 13 (2000) 67.
[52] J.M. Thomas, B.F.G. Johnson, R. Raja, G. Sankar, P.A. Midgley, Acc. Chem. Res. 36 (2003) 20.
[53] I.E. Wachs, Top. Catal. 8 (1999) 57.
[54] I.E. Wachs, Surf. Sci. 544 (2003) 1.
[55] S. Bertarione, D. Scarano, A. Zecchina, V. Johanek, J. Hoffmann, S. Schauermann, M. Frank, J. Libuda, G. Rupprechter, H.-J. Freund, J. Phys. Chem. B 108 (2004) 3603.
[56] S. Sao-Joao, S. Giorgio, J. Penisson, C. Chapon, S. Bourgeois, C.R. Henry, J. Phys. Chem. B 109 (2005) 342.
[57] T. Lear, R. Marshall, E.K. Gibson, T. Schütt, T.M. Klapötke, G. Rupprechter, H.-J. Freund, J.M. Winfield, D. Lennon, Phys. Chem. Chem. Phys. 7 (2005) 565.
[58] T. Lear, R. Marshall, J.A. Lopez-Sanchez, S.D. Jackson, T.M. Klapötke, M. Bäumer, G. Rupprechter, H.-J. Freund, D. Lennon, J. Chem. Phys. 123 (2005) 174706.
[59] J.M. Thomas, G.A. Somorjai (Eds.), Topics in Catalysis, Special Issue on In situ Characterization of Catalysts, 1999.
[60] R. Schlögl, A. Zecchina (Eds.), Topics in Catalysis, Special Issue on In situ Characterization of Catalysts, 2001.
[61] T. Hansen, J. Wagner, P. Hansen, S. Dahl, H. Topsoe, C. Jacobsen, Science 294 (2001) 1508.
[62] J.M. Thomas, P.L. Gai, Adv. Catal. 48 (2004) 171.
[63] S. Giorgio, S. Sao Joao, S. Nitsche, D. Chaudanson, G. Sitja, C.R. Henry, Ultramicroscopy 106 (2006) 503.
[64] Y.R. Shen, Surf. Sci. 299–300 (1994) 551.
[65] A. Tadjeddine, A. Peremans, Surf. Sci. 368 (1996) 377.
[66] C.T. Williams, D.A. Beattie, Surf. Sci. 500 (2002) 545.
[67] B.J. Barner, M.J. Green, E.I. Saez, R.M. Corn, Anal. Chem. 63 (1991).
[68] G.A. Beitel, A. Laskov, H. Oosterbeek, E.W. Kuipers, J. Phys. Chem. 100 (1996) 12494.
[69] D. Stacchiola, A. Thompson, G. Kaltchev, W.T. Tysoe, J. Vac. Sci. Technol. A 20 (2002) 2101.
[70] Y. Jugnet, F.J. Cadete Santos Aires, C. Deranlot, L. Piccolo, J.C. Bertolini, Surf. Sci. 521 (2002) L639.
[71] E. Ozensoy, D. Meier, D. Goodman, J. Phys. Chem. B. 106 (2002) 9367.
[72] O. Rodríguez de la Fuente, M. Borasio, P. Galletto, G. Rupprechter, H.-J. Freund, Surf. Sci. 566–568 (2004) 740.
[73] M. Andersen, M. Johansson, I. Chorkendorff, J. Phys. Chem. B. 109 (2005) 10285.
[74] M. Borasio, O. Rodríguez de la Fuente, G. Rupprechter, H.-J. Freund, J. Phys. Chem. B Lett. 109 (2005) 17791.
[75] G. Rupprechter, T. Dellwig, H. Unterhalt, H.-J. Freund, J. Phys. Chem. B 105 (2001) 3797.
[76] F.M. Hoffmann, Surf. Sci. Rep. 3 (1983) 103.
[77] L.T. Richter, T.P. Petrallimallow, J.C. Stephenson, Opt. Lett. 23 (1998) 1594.
[78] E.W.M. van der Ham, Q.H.F. Vrehen, E.R. Eliel, Surf. Sci. 368 (1996) 96.
[79] H. Ueba, Prog. Surf. Sci. 55 (1997) 115.
[80] M. Bonn, C. Hess, S. Funk, J. Miners, B.N.J. Persson, M. Wolf, G. Ertl, Phys. Rev. Lett. 84 (2000) 4653.
[81] A. Bandara, S. Dobashi, J. Kubota, K. Onda, A. Wada, K. Domen, C. Hirose, S. Kano, Surf. Sci. 387 (1997) 312.
[82] P. Galletto, H. Unterhalt, G. Rupprechter, Chem. Phys. Lett. 367 (2003) 785.
[83] M. Morkel, H. Unterhalt, T. Klüner, G. Rupprechter, H.-J. Freund, Surf. Sci. 586 (2005) 146.
[84] E.H.G. Backus, M. Bonn, Chem. Phys. Lett. 412 (2005) 152.
[85] K.Y. Kung, P. Chen, F. Wei, G. Rupprechter, Y.R. Shen, G.A. Somorjai, Rev. Sci. Instrum. 72 (2001) 1806.
[86] G. Rupprechter, M. Morkel, H.-J. Freund, R. Hirschl, Surf. Sci. 554 (2004) 43.
[87] K. Wolter, O. Seiferth, H. Kuhlenbeck, M. Bäumer, H.-J. Freund, Surf. Sci. 399 (1998) 190.
[88] H. Unterhalt, Ph.D. thesis, Free University Berlin, 2002.
[89] A.K. Datye, D.J. Smith, Catal. Rev.-Sci. Eng. 34 (1992) 129.
[90] S. Bernal, J.J. Calvino, M.A. Cauqui, J.M. Gatica, C. Larese, J.A. Perez-Omil, J.M. Pintado, Catal. Today 50 (1999) 175.
[91] I.V. Yudanov, R. Sahnoun, K.M. Neyman, N. Rösch, J. Hoffmann, S. Schauermann, V. Johánek, H. Unterhalt, G. Rupprechter, L. Libuda, H.-J. Freund, J. Phys. Chem. B. 107 (2003) 255.
[92] P. Hollins, Surf. Sci. Rep. 16 (1992) 51.
[93] M. Morkel, G. Rupprechter, H.-J. Freund, Surf. Sci. Lett. 588 (2005) L209.
[94] G. Rupprechter, G.A. Somorjai, Catal. Lett. 48 (1997) 17.
[95] S.T. Ceyer, Acc. Chem. Res. 34 (2001) 737.
[96] A. Doyle, S. Shaikhutdinov, S.D. Jackson, H.-J. Freund, Angew. Chem. Int. Ed. Engl. 42 (2003) 5240.
[97] M. Morkel, G. Rupprechter, H.-J. Freund, J. Chem. Phys. 119 (2003) 10853.
[98] M. Morkel, H. Unterhalt, M. Salmeron, G. Rupprechter, H.-J. Freund, Surf. Sci. 532–535 (2003) 103.
[99] M.K. Rose, T. Mitsui, J. Dunphy, A. Borg, D.F. Ogletree, M. Salmeron, P. Sautet, Surf. Sci. 512 (2002) 48.
[100] S. Surnev, M. Sock, M.G. Ramsey, F.P. Netzer, M. Wiklund, M. Borg, J.N. Andersen, Surf. Sci. 470 (2000) 171.
[101] T. Mitsui, M.K. Rose, E. Fomin, D.F. Ogletree, M. Salmeron, Nature 422 (2003) 705.
[102] M. Neurock, Top. Catal. 9 (1999) 135.
[103] G. Rupprechter, V.V. Kaichev, H. Unterhalt, M. Morkel, V.I. Bukhtiyarov, Appl. Surf. Sci. 235 (2004) 26.
[104] V.V. Kaichev, M. Morkel, H. Unterhalt, I.P. Prosvirin, V.I. Bukhtiyarov, G. Rupprechter, H.-J. Freund, Surf. Sci. 566–568 (2004) 1024.
[105] C. Chinchen, P.J. Denny, J.R. Jennings, M.S. Spencer, K.C. Waugh, Appl. Catal. 36 (1988) 1.
[106] A.F. Gusovius, T.C. Watling, R. Prins, Appl. Catal. A 188 (1999) 187.
[107] M.A. Vannice, Catal. Rev. Sci. Eng. 14 (1976) 153.
[108] M. Morkel, V.V. Kaichev, G. Rupprechter, H.-J. Freund, I.P. Prosvirin, V.I. Bukhtiyarov, J. Phys. Chem. B. 108 (2004) 12955.
[109] M. Mavrikakis, M.A. Barteau, J. Mol. Catal. A 131 (1998) 135.
[110] C. Sellmer, R. Prins, N. Kruse, Catal. Lett. 47 (1997) 83.
[111] R.F. Hicks, A.T. Bell, J. Catal. 90 (1984) 205.
[112] K. Christmann, J.E. Demuth, J. Chem. Phys. 76 (1982) 6308.
[113] G.A. Kok, A. Noordermeer, B.E. Nieuwenhuys, Surf. Sci. 135 (1983) 65.
[114] J.A. Gates, L.L. Kesmodel, J. Catal. 83 (1983) 437.
[115] X. Guo, L. Hanley, J.T. Yates, J. Am. Chem. Soc. 111 (1989) 3155.
[116] J.L. Davis, M.A. Barteau, Surf. Sci. 235 (1990) 235.
[117] S.M. Francis, J. Corneille, D.W. Goodman, M. Bowker, Surf. Sci. 364 (1996) 30.
[118] R.J. Levis, J. Zhicheng, N. Winograd, J. Am. Chem. Soc. 111 (1989) 4605.
[119] J.-J. Chen, Z.-C. Jiang, Y. Zhou, B.R. Chakraborty, N. Winograd, Surf. Sci. 328 (1995) 248.
[120] N. Kruse, M. Rebholz, V. Matolin, G.K. Chuah, J.H. Block, Surf. Sci. 238 (1990) L457.
[121] M. Rebholz, N. Kruse, J. Chem. Phys. 95 (1991) 7745.

[122] S. Schauermann, J. Hoffmann, V. Johánek, J. Hartmann, J. Libuda, H.-J. Freund, Catal. Lett. 84 (2002) 209.
[123] R. Schennach, A. Eichler, K.D. Rendulic, J. Phys. Chem. B. 107 (2003) 2552.
[124] C.J. Zhang, P. Hu, J. Chem. Phys. 115 (2001) 7182.
[125] M. Borasio, M. Morkel, G. Rupprechter, H.-J. Freund, in preparation, 2007.
[126] G. Rupprechter, H. Unterhalt, M. Borasio, M. Morkel, H.-J. Freund, Annu. Rep. Max Planck Soc. (Jahrb.) (2005) 193.
[127] R.B. Barros, A.R. Garcia, L.M. Ihlarco, J. Phys. Chem. B 105 (2001) 11186.
[128] M. Endo, T. Matsumoto, J. Kubota, K. Domen, C. Hirose, J. Phys. Chem. B 105 (2001) 1573.
[129] W.J. Mitchell, J. Xie, T.A. Jachimowski, W.H. Weinberg, J. Am. Chem. Soc. 117 (1995) 2606.
[130] J.L. Davis, M.A. Barteau, J. Am. Chem. Soc. 111 (1989) 1782.
[131] I.V. Yudanov, K.M. Neyman, N. Rösch, Phys. Chem. Chem. Phys. 6 (2004) 116.
[132] S.K. Desai, M. Neurock, K. Kourtakis, J. Phys. Chem. B 106 (2002) 2559.
[133] S. Stolbov, F. Mehmood, T.S. Rahman, M. Alatalo, I. Makkonen, P. Salo, Phys. Rev. B 70 (2004) 155410.
[134] F.P. Leisenberger, G. Koller, M. Sock, S. Surnev, M.G. Ramsey, F.P. Netzer, B. Klötzer, K. Hayek, Surf. Sci. 445 (2000) 380.
[135] E. Lundgren, G. Kresse, C. Klein, M. Borg, J.N. Andersen, M. De Santis, Y. Gauthier, C. Konvicka, M. Schmid, P. Varga, Phys. Rev. Lett. 88 (2002) 246103.
[136] E. Lundgren, J. Gustafson, A. Mikkelsen, J.N. Andersen, A. Stierle, H. Dosch, M. Todorova, J. Rogal, K. Reuter, M. Scheffler, Phys. Rev. Lett. 92 (2004) 046101.
[137] H. Over, Y.D. Kim, A.P. Seitsonen, S. Wendt, E. Lundgren, M. Schmid, P. Varga, A. Morgante, G. Ertl, Science 287 (2000) 1474.
[138] K. Reuter, M. Scheffler, Phys. Rev. B 65 (2001) 035 406.
[139] S.H. Kim, J. Wintterlin, J. Phys. Chem. B 108 (2004) 14565.
[140] O. Demoulin, G. Rupprechter, I. Seunier, B.L. Clef, M. Navez, P. Ruiz, J. Phys. Chem. B 109 (2005) 20454.
[141] M. Borasio, PhD thesis, Free University Berlin, 2006.
[142] M. Bäumer, J. Libuda, K.M. Neyman, N. Rösch, G. Rupprechter, H.-J. Freund, Phys. Chem. Chem. Phys., submitted for publication.
[143] T. Schalow, M. Laurin, B. Brandt, S. Schauermann, S. Guimond, H. Kuhlenbeck, D.E. Starr, S.K. Shaikhutdinov, J. Libuda, H.-J. Freund, Angew. Chem. Int. Ed. 44 (2005) 2.
[144] T. Schalow, B. Brandt, M. Laurin, S. Schauermann, J. Libuda, H.-J. Freund, J. Catal. 242 (2006) 58.
[145] H. Gabasch, A. Knop-Gericke, R. Schlögl, M. Borasio, C. Weilach, G. Rupprechter, S. Penner, B. Jenewein, K. Hayek, B. Klötzer, Phys. Chem. Chem. Phys. 9 (2007) 533.
[146] H. Kuhlenbeck, H.-J. Freund, in: H.P. Bonzel (Ed.), Landolt-Börnstein: Physics of Covered Solid Surfaces, III-42, Springer, 2006, p. 332.
[147] F. Höbel, A. Bandara, G. Rupprechter, H.-J. Freund, Surf. Sci. 600 (2006) 963.
[148] J. Middeke, R.-P. Blum, M. Hafemeister, H. Niehus, Surf. Sci. 587 (2005) 219.
[149] D.E. Starr, F.M.T. Mendes, J. Middeke, R.-P. Blum, H. Niehus, D. Lahav, S. Guimond, A. Uhl, T. Klüner, M. Schmal, H. Kuhlenbeck, S. Shaikhutdinov, H.-J. Freund, Surf. Sci. 599 (2005) 14.
[150] F.M.T. Mendes, A. Uhl, D.E. Starr, S. Guimond, M. Schmal, H. Kuhlenbeck, S. Shaikhutdinov, H.-J. Freund, Catal. Lett. 111 (2006) 35.
[151] F.M.T. Mendes, C.A.C. Perez, F.B. Noronha, M. Schmal, Catal. Today 101 (2005) 45.
[152] J. Silvestre-Albero, G. Rupprechter, H.-J. Freund, Chem. Commun. (2006) 80.
[153] J. Silvestre-Albero, G. Rupprechter, H.-J. Freund, J. Catal. 240 (2006) 58.
[154] B. Tardy, C. Noupa, C. Leclercq, J.C. Bertolini, A. Hoareau, M. Treilleux, J.P. Faure, G. Nihoul, J. Catal. 129 (1991) 1.
[155] J. Massardier, J.C. Bertolini, A. Renouprez, in: Proceedings of the 9th International Congress on Catalysis, vol. 3, Calgary, (1988), p. 1222.
[156] J. Silvestre-Albero, G. Rupprechter, H.-J. Freund, J. Catal. 235 (2005) 52.
[157] J. Silvestre-Albero, M. Borasio, G. Rupprechter, H.-J. Freund, Catal. Commun. 8 (2007) 292.